Relativistic free-electron dynamics and light-emission spectra in the simultaneous presence of a superintense laser field and a strong uniform magnetic field

Yousef I. Salamin*
Physics Department, Birzeit University, P. O. Box 14, Birzeit, West Bank

Farhad H. M. Faisal
Fakultät für Physik, Universität Bielefeld, 33615 Bielefeld, Germany
(Received 22 January 1998; revised manuscript received 28 August 1998)

We present exact analytic trajectories for a relativistic electron in the presence of an elliptically polarized superintense laser field *and* a strong uniform magnetic field. Also derived are expressions for the velocity components of the electron and for its energy as functions of the phase of the laser field as a parameter. The analytic trajectory solutions are illustrated by numerical calculations employing laser-field parameters and magnetic-field strengths currently available for laboratory experiments. The trajectory solutions are useful for (among other things) the study of the related problem of emission of radiation in the combined laser and magnetic fields. An exact expression for the cross section of light scattered by an electron initially moving along the laser propagation direction and in a magnetic field is given. It is found that, for observation along the common direction of laser propagation and the magnetic field, light at two frequencies $\omega=\omega_0$ and Ω_0 is scattered, where $\Omega_0=\gamma_0(1+\beta_0)\omega_c$, ω_c is the cyclotron frequency of the electron motion in the magnetic field, β_0 is the initial speed of the electron normalized by the speed of light, $\gamma_0=(1-\beta_0^2)^{-1/2}$, and ω_0 is the laser frequency. Using the analytic solutions, we also study numerically the spectrum of radiation emitted along observation directions parallel to the electric and parallel to the magnetic components of the laser field. In each case, we present and discuss the dependence of the spectra on (a) the increase of the electron initial velocity, (b) the intensity and the frequency of the laser, and (c) the strength of the magnetic field. [S1050-2947(98)09409-8]

PACS number(s): 42.65.Ky, 52.40.Nk, 42.50.Vk, 52.75.Di

I. INTRODUCTION

In a series of papers [1–4] we have recently studied the problem of generation of radiation by the scattering of superintense laser light from fast free electrons. We have studied analytically the electron dynamics as well as the light emission cross sections corresponding to linearly and circularly polarized incident light. In the present paper we investigate similar physical situations, but with the added feature of a strong uniform magnetic field parallel to the laser propagation direction. This problem is important for the understanding of laser-plasma interactions and the related problems of high-energy electron emission [5–7], as well as for the interpretation and understanding of current laser-assisted fusion experiments [8].

The problem of harmonic generation (or, more generally, emission of radiation) due to the interaction of an atomic electron with a superintense laser field has been the subject of recent theoretical investigations, via Monte Carlo classical simulations, by Keitel and Knight [9]. They studied numerically the trajectories and harmonic spectra of an electron initially bound in a ground-state hydrogen atom, within various approximations that they described in their paper. An interesting finding of their simulations is that the results obtained in the case of an (initially) free electron hardly differed from their counterparts for an initially bound hydrogenic electron subjected to a strong magnetic field and a superintense laser field. This is because, for field intensities greater than 1 a.u. $I_0\approx 3.51\times 10^{16}$ W/cm^2, the force of the laser becomes stronger than the binding force of the nucleus, and hence the resulting dynamics tends to resemble that of a free electron [10] in superintense fields. In a more recent paper, Connerade and Keitel [11] have investigated the same problem for an initially bound electron, but in the added presence of a strong uniform magnetic field, again employing Monte Carlo simulations. In their paper the authors also make a remark to the effect that pulsed magnetic fields of strength up to 75 T (and laser-field intensities in excess of 10^{16} W/cm^2, needed for such experiments) have been realized in their laboratory. Magnetic fields of such strength were realized by Foner and Kolm [12] a long time ago.

The main purpose of this paper is to derive and present exact analytic solutions for the fully relativistic electron trajectories in the presence of a superintense plane-wave laser field *and* a strong uniform magnetic field and to illustrate their usefulness by considering the generation of radiation. The scattered radiation cross sections are also obtained analytically for the case of observation along the laser direction of propagation. The use of the trajectories derived here is further illustrated by calculating (by quadrature of the relevant formulas) the emission spectra to be observed along the transverse directions. The trajectories in the laser and magnetic fields are found to differ significantly from those obtained in the absence of a magnetic field. Thus, for ex-

*Corresponding address: Physics Department, Birzeit University, P.O. Box 14, Birzeit, West Bank, via Israel.

ample, it is found that for a field strength $B_0 \approx 30$ T, currently available [11,12], the electron follows a helical trajectory (with its axis along the direction of the magnetic field) with *superimposed* little wiggles on it. The presence of the wiggles on the trajectory is expected to lead, in general, to rich structures in the emission spectra, although for specific geometries it may give a simple spectrum. An example of a simple emission spectrum is obtained in the case in which the initial electron motion is parallel to the magnetic-field direction and the scattered light is also along that direction. It is found that the emission occurs at two frequencies, namely, at the fundamental frequency $\omega = \omega_0$ and at $\omega = \Omega_0$, where ω_0 is the frequency of the laser and Ω_0 (to be defined explicitly below) depends on the magnetic-field strength. Such a line has been found by a Monte Carlo simulation [11]. We note that, in the absence of B_0, one gets only the fundamental frequency $\omega = \omega_0$ in the forward direction. As further illustrations of the use of the analytic solutions derived here, we also study the emission spectra for observation directions along the electric- and magnetic-field components of the laser field. These spectra are evaluated by quadrature of the cross-section formula using the experessions of the trajectories. The dependence of the spectra on the initial electron kinetic energy, on the laser intensity and frequency, and on the strength of the uniform magnetic field is obtained and discussed.

Below we also consider the so-called ponderomotive scattering in the presence of a magnetic field. Specifically, expressions for the dependence, on the field parameters, of the scattering angle of the electron θ relative to the laser direction of propagation and an appropriate azimuth angle ϕ are derived. It is shown that θ depends only on the laser-field parameters (not on the magnetic field), whereas the azimuth ϕ depends on the magnetic field as well, as might be expected [3].

The rest of the paper is organized as follows. In Sec. II parametric equations, employing the phase of the laser field as a parameter, for the relativistic trajectory of an electron in the presence of both the laser and the magnetic fields are derived. In Sec. III explicit expressions for the velocity components of the electron, its energy, and the ponderomotive scattering angles are given for the special case in which the electron initially moves along the direction of propagation of a linearly polarized laser field. In the same section we show graphically the electron trajectories, velocity components, and energy for two cases of laser-field polarization. In Sec. IV a general expression for the light-emission cross section will be given, which will also be the starting point for derivations involving special cases in the Appendixes. Emission spectra calculated numerically on the basis of the general expression will be presented and discussed for a number of cases in this section too. The corresponding expression for the case of circular polarization of the laser will also be given. We conclude by giving a brief discussion of the results obtained, in Sec. V.

II. ELECTRON DYNAMICS

The relativistic motion of an electron in the presence of plane wave and pulsed laser fields is well understood [1,2,13]. About ten years ago Kyrala [14] gave a numerical study of the motion of a (hydrogen) atomic electron after ionization in the field of an intense laser pulse, using a classical model for the binding potential. More recently, Connerade and Keitel [11] presented the results of a numerical calculation of the trajectory of the same system, in the added presence of a strong magnetic field pointing along the direction of laser-field propagation, within the context of their study of high harmonic generation. It has been concluded from these studies that, in very intense laser fields, the dynamics of the ionized electron differs in no significant way from that of an initially free electron. In this section we derive analytic trajectories for a *free* electron in a plane-wave laser field *and* a strong magnetic field.

A. Preliminaries

We wish to study the motion of, and the scattering of radiation from, a relativistic electron, of mass m and charge $-e$, in the simultaneous presence of an intense plane-wave laser field and a strong uniform magnetic field. The energy-momentum four-vector of the electron will be denoted by $p = (\mathcal{E}/c, \mathbf{p})$, where

$$\mathcal{E} = \gamma m c^2, \quad \mathbf{p} = \gamma m c \boldsymbol{\beta}. \tag{1}$$

In Eq. (1), $\boldsymbol{\beta}$ is the electron velocity normalized by c, the speed of light, and $\gamma = (1-\beta^2)^{-1/2}$. The electric and magnetic fields will be derived from a vector potential $\mathbf{A}$ via the equations

$$\mathbf{E} = -\frac{1}{c}\frac{\partial \mathbf{A}}{\partial t}, \quad \boldsymbol{B} = \nabla \times \mathbf{A}. \tag{2}$$

The dynamics of the electron will be studied on the basis of the energy-momentum transfer equations

$$\frac{d\mathbf{p}}{dt} = -e(\mathbf{E} + \boldsymbol{\beta} \times \mathbf{B}) \tag{3}$$

and

$$\frac{d\mathcal{E}}{dt} = -ec\boldsymbol{\beta} \cdot \mathbf{E}. \tag{4}$$

B. General

In this subsection we develop the electron dynamics resulting from interaction with a superintense plane-wave laser field and a strong uniform magnetic field aligned in the direction of propagation of the laser field. The vector potential in the present situation is given by

$$\mathbf{A} = A_0[\hat{\mathbf{i}}\delta\cos\eta + \hat{\mathbf{j}}\sqrt{1-\delta^2}\sin\eta] - \frac{B_0}{2}(\hat{\mathbf{i}}y - \hat{\mathbf{j}}x). \tag{5}$$

The first term in Eq. (5) represents a plane-wave, elliptically polarized laser field of peak field strength A_0, frequency ω_0, and wave vector $\mathbf{k}$ pointing in the positive coordinate z direction. The second term represents a magnetic field of constant magnitude B_0 and direction also along z. Furthermore, the phase of the field η stands for the invariant combination

$\omega_0 t - \mathbf{k}\cdot\mathbf{r}$ and δ gives the degree of ellipticity (with $\delta=1$ for linear and $\delta=1/\sqrt{2}$ for circular polarizations).

Using Eq. (5) in Eqs. (3) and (4), we get the equations of motion

$$\frac{d(\gamma\beta_x)}{dt} = -q\delta\omega_0(1-\beta_z)\sin\eta - \omega_c\beta_y, \tag{6}$$

$$\frac{d(\gamma\beta_y)}{dt} = q\sqrt{1-\delta^2}\,\omega_0(1-\beta_z)\cos\eta + \omega_c\beta_x, \tag{7}$$

$$\frac{d(\gamma\beta_z)}{dt} = q\omega_0[\sqrt{1-\delta^2}\beta_y\cos\eta - \delta\beta_x\sin\eta], \tag{8}$$

$$\frac{d\gamma}{dt} = q\omega_0[\sqrt{1-\delta^2}\beta_y\cos\eta - \delta\beta_x\sin\eta], \tag{9}$$

where $\omega_c = eB_0/mc$ is the cyclotron frequency of the electron motion in the magnetic field B_0 and $q=eA_0/mc^2$ is the dimensionless intensity parameter of the laser field ($q=1$ corresponds to a laser intensity of $I\approx 10^{18}$ W/cm^2). Note that the right-hand sides of Eqs. (8) and (9) are identical, so if we equate the left-hand sides and carry out the single integration, we arrive at the useful relation

$$\gamma(1-\beta_z) = \gamma_0(1-\beta_{z0}), \tag{10}$$

where the subscript 0 signifies an initial value, at $t=0$, for the quantity in question. Another useful relation may be obtained from differentiating the phase η once with respect to time

$$\frac{d\eta}{dt} = \omega_0(1-\beta_z). \tag{11}$$

A third relation, which will prove to be important for the calculation of the electron trajectories below, can be obtained by considering the derivative of a typical Cartesian coordinate with respect to the phase η, aided by Eqs. (10) and (11). With Q standing for $x,y,$ or z, we have

$$\frac{dQ}{d\eta} = \frac{dQ}{dt}\frac{dt}{d\eta} = \frac{c}{\omega_0}\frac{\gamma\beta_Q}{\gamma_0(1-\beta_{z0})}. \tag{12}$$

The following (fourth) relation may also be derived as indicated below with relative ease,

$$\gamma^2(\beta_x^2+\beta_y^2) - \gamma_0^2(\beta_{x0}^2+\beta_{y0}^2) = 2\gamma_0(1-\beta_{z0})(\gamma-\gamma_0). \tag{13}$$

The steps leading to Eq. (13) are as follows. First Eq. (6) is multiplied through by $\gamma\beta_x$ and the resulting equation is then added to Eq. (7) times $\gamma\beta_y$. The result is then rearranged and use is made of Eqs. (10) and (9). Finally, a single integration yields Eq. (13).

We are now in a position to calculate the exact electron trajectories. Using Eq. (11) in the first term on the right hand side of Eq. (6) and writing $\beta_y = dy/cdt$ in the second results in a simple differential equation. A single integration then yields

$$\gamma\beta_x = \gamma_0\beta_{x0} + q\delta(\cos\eta - \cos\eta_0) - \frac{\omega_c}{c}(y-y_0). \tag{14}$$

Similarly,

$$\gamma\beta_y = \gamma_0\beta_{y0} + q\sqrt{1-\delta^2}(\sin\eta - \sin\eta_0) + \frac{\omega_c}{c}(x-x_0). \tag{15}$$

Using Eqs. (14) and (15) in Eq. (12) results in the following coupled differential equations for x and y, respectively,

$$\frac{dx}{d\eta} = \frac{c}{\omega_0\gamma_0(1-\beta_{z0})}\left[q\delta(\cos\eta-\cos\eta_0) - \frac{\omega_c}{c}(y-y_0) + \gamma_0\beta_{x0}\right], \tag{16}$$

$$\frac{dy}{d\eta} = \frac{c}{\omega_0\gamma_0(1-\beta_{z0})}\left[q\sqrt{1-\delta^2}(\sin\eta-\sin\eta_0) + \frac{\omega_c}{c}(x-x_0) + \gamma_0\beta_{y0}\right]. \tag{17}$$

When Eq. (17) is multiplied by i and the result is added to Eq. (16), a simple first order differential equation for the quantity $\rho = x+iy$ results. The solution of this equation may best be achieved by an integrating factor. The idea is to cast the equation into the form

$$\frac{d\rho}{d\eta} + P(\eta)\rho = R(\eta), \tag{18}$$

whose solution may be written as

$$\rho = e^{-I(\eta)}\left\{\int^{\eta} R(\eta')e^{I(\eta)}d\eta' + C\right\}, \tag{19}$$

where $I(\eta) = \int^{\eta} P(\eta')d\eta'$ and C is a complex constant to be determined from the initial conditions. The real and imaginary parts of ρ finally give expressions for $x(\eta)$ and $y(\eta)$, respectively. After some lengthy algebra, we get

$$x(\eta) = \frac{qc}{\omega_0\gamma_0(1-\beta_{z0})}\left[\frac{\delta + r\sqrt{1-\delta^2}}{1-r^2}\right]\sin\eta + \frac{c}{\omega_0\gamma_0(1-\beta_{z0})} \times\left[\frac{-\gamma_0\beta_{y0} + \frac{\omega_c}{c}x_0 + q\sqrt{1-\delta^2}\sin\eta_0}{r}\right] + a\cos(r\eta) - b\sin(r\eta), \tag{20}$$

$$y(\eta) = -\frac{qc}{\omega_0\gamma_0(1-\beta_{z0})}\left[\frac{r\delta + \sqrt{1-\delta^2}}{1-r^2}\right]\cos\eta + \frac{c}{\omega_0\gamma_0(1-\beta_{z0})}\left[\frac{\gamma_0\beta_{x0} + \frac{\omega_c}{c}y_0 - q\delta\cos\eta_0}{r}\right] + a\sin(r\eta) + b\cos(r\eta). \tag{21}$$

In Eqs. (20) and (21), a and b are the real and imaginary parts, respectively, of the constant C and r stands for the frequency ratio

$$r=\Omega_0/\omega_0=\frac{\omega_c/\omega_0}{\gamma_0(1-\beta_{z0})}. \tag{22}$$

Ω_0 may be thought of as a *reduced cyclotron frequency* for the relativistic electron motion in the magnetic field. An alternative way of arriving at Eqs. (20) and (21) would be to decouple Eqs. (16) and (17) by differentiating one of them once more with respect to η and then using the other one to get a second-order ordinary differential equation whose solution may then be found using standard techniques.

Our equations, derived so far in most generality, constitute a set of basic working expressions from which a full account of the electron motion, in the intense plane-wave laser field and strong magnetic field, may be made. The expressions for $\gamma\beta_x$ and $\gamma\beta_y$ are again given by Eqs. (14) and (15), respectively, where x and y are now given by $x(\eta)$ and $y(\eta)$ as shown in Eqs. (20) and (21), respectively. An analytic expression for the Lorentz factor γ, and hence the electron energy γmc^2, may also be found by substituting the expressions found for $\gamma\beta_x$ and $\gamma\beta_y$ in Eq. (13). The expression for γ, thus obtained, may then be used in Eq. (10) in order to obtain $\beta_z(\eta)$. Finally, when $\gamma\beta_z$ is used in Eq. (12) for $Q=z$ and after the integration over η has been carried out, one obtains $z(\eta)$. With $z(\eta)$ known, the set of parametric equations giving the particle trajectory in terms of the parameter η is complete. We now elect to apply the above results to a specialized situation corresponding to a specific set of initial conditions on the electron position and velocity vectors and work through it in detail.

III. INITIAL MOTION PARALLEL TO THE PROPAGATION DIRECTION OF A LINEARLY POLARIZED FIELD

This section is devoted to a detailed study of the dynamics of an electron initially moving parallel to the laser propagation direction at the speed $v_{z0}=c\beta_0$. We take the zero of time at the instant the electron passes the origin of coordinates. Thus the initial position of the electron corresponds to $x_0=y_0=z_0=0$ and the initial velocity is given by $\beta_{x0}=\beta_{y0}=0$ and $\beta_{z0}=\beta_0$. This choice of initial conditions implies $\eta_0=0$ and $\gamma_0=(1-\beta_0^2)^{-1/2}$. Let us specialize further to the case of a linearly polarized laser field with $\delta=1$. This situation has been studied recently in the absence of the applied strong magnetic field. So we shall have the chance to compare our equations and other results for the electron trajectory with those of Refs. [2,3,15] in the limit of $r\rightarrow 0$.

A. Equations

Using the above-mentioned initial conditions in Eqs. (20) and (21) fixes the values of the constants a and b. In this case, $a=0$ and $b=(qc/\omega_0)\gamma_0(1+\beta_0)/r(1-r^2)$. This result, together with algebraic manipulations along the lines sketched at the end of Sec. II, lead to the trajectory equations

$$x(\eta)=\frac{\lambda}{2\pi}q\gamma_0(1+\beta_0)\left[\frac{r\sin\eta-\sin(r\eta)}{r(1-r^2)}\right], \tag{23}$$

$$y(\eta)=\frac{\lambda}{2\pi}q\gamma_0(1+\beta_0)\left[\frac{-r^2\cos\eta+\cos(r\eta)+r^2-1}{r(1-r^2)}\right], \tag{24}$$

$$z(\eta)=\frac{\lambda}{2\pi}\left(\frac{1+\beta_0}{1-\beta_0}\right)\left\{\left[\frac{\beta_0}{1+\beta_0}+\frac{q^2}{4}\frac{3+r^2}{(1-r^2)^2}\right]\eta+\frac{q^2}{8}\frac{\sin(2\eta)}{(1-r^2)}-\frac{q^2}{2}\left[\frac{(1+r)^2\sin[(1-r)\eta]+(1-r)^2\sin[(1+r)\eta]}{(1-r^2)^3}\right]\right\}, \tag{25}$$

where λ is the laser field wavelength. In the absence of the applied strong magnetic field B_0, these equations exactly reproduce the results of Hartemann *et al.* [15]. To show this, one simply takes the limit as $r\rightarrow 0$ in Eqs. (23)–(25), employing l'Hospital's rule in Eqs. (23) and (24).

Next, we use the same initial conditions, together with Eqs. (23)–(25), in Eqs. (14) and (15) in order to find expressions for $\gamma\beta_x$ and $\gamma\beta_y$. Furthermore, an expression for $\gamma\beta_z$ follows from Eq. (10). Thus the components of the electron velocity vector $\boldsymbol{\beta}(\eta)$ are found to be

$$\beta_x(\eta)=\frac{q}{\gamma(\eta)}\left[\frac{\cos\eta-\cos(r\eta)}{1-r^2}\right], \tag{26}$$

$$\beta_y(\eta)=\frac{q}{\gamma(\eta)}\left[\frac{r\sin\eta-\sin(r\eta)}{1-r^2}\right], \tag{27}$$

$$\beta_z(\eta)=\frac{\gamma_0}{\gamma(\eta)}\left\{\beta_0+\frac{1}{2}q^2(1+\beta_0)\left[\frac{[\cos\eta-\cos(r\eta)]^2+[r\sin\eta-\sin(r\eta)]^2}{(1-r^2)^2}\right]\right\}, \tag{28}$$

where the Lorentz factor, or the electron energy scaled by the rest energy mc^2, is

$$\gamma(\eta)=\gamma_0\left\{1+\frac{1}{2}q^2(1+\beta_0)\left[\frac{[\cos\eta-\cos(r\eta)]^2+[r\sin\eta-\sin(r\eta)]^2}{(1-r^2)^2}\right]\right\}. \quad (29)$$

Again, Eqs. (26)–(29) reproduce the known results in the absence of the applied magnetic field ($r\to 0$) [15]. Note also that, viewed as a function of the phase η, the scaled energy oscillates between a minimum value of $\gamma_{min}\approx\gamma_0$ and a maximum value of $\gamma_{max}\approx\gamma_0\{1+2q^2(1+\beta_0)\}$, as the electron interacts with the applied laser field.

We would like to make the remark, at this point, that simpler expressions corresponding to Eqs. (23)–(29) may be arrived at very easily for the case of a circularly polarized laser field. The results will be shown only in graphical form in Sec. III B.

We close this subsection by deriving expressions for the ponderomotive scattering angles of the electron in terms of its escape kinetic energy and other parameters relevant to the initial conditions of interest. The angle θ, measured relative to the z axis, is given by

$$\theta(\gamma)=\tan^{-1}\left\{\frac{\sqrt{(\beta_x)^2+(\beta_y)^2}}{\beta_z}\right\}$$
$$=\tan^{-1}\left\{\frac{\sqrt{\frac{2}{1+\beta_0}\left(\frac{\gamma}{\gamma_0}-1\right)}}{\gamma-\gamma_0(1-\beta_0)}\right\}. \quad (30)$$

The easiest way to arrive at Eq. (30) is by using Eqs. (13) and (10) after the initial conditions have been inserted in both. Equation (30) is identical to the expression reported recently by Hartemann *et al.* [15] without the added B_0 field. In terms of the escape kinetic energy $K=(\gamma-1)mc^2$ where γ is given in Eq. (29), the scattering angle is given by

$$\theta(K)=\tan^{-1}\left\{\frac{\sqrt{2(1-\beta_0)(K-K_0)/\gamma_0 mc^2}}{\beta_0+(K-K_0)/\gamma_0 mc^2}\right\}, \quad (31)$$

where $K_0=(\gamma_0-1)mc^2$ is the initial kinetic energy with which the electron is injected into the field. An equation with the same functional dependence on K as Eq. (31) has also recently been derived by us [1,2] in the absence of the field B_0.

The added magnetic field B_0 will alter the azimuthal angle ϕ, measured in the present situation relative to the x axis. The expression for ϕ is

$$\phi=\tan^{-1}\left(\frac{\beta_y}{\beta_x}\right)$$
$$=\tan^{-1}\left\{\frac{r\sin\eta-\sin(r\eta)}{\cos\eta-\cos(r\eta)}\right\}. \quad (32)$$

Note that in the absence of the added magnetic field $r=0$, Eq. (32) yields $\phi=0$. In this case, the electron motion is entirely confined to the xz plane. We have recently obtained the same expression as well, using a different approach [2].

B. Numerical analysis

Some of the analytical results obtained so far will now be shown in graphical form. We will show the actual trajectory of the electron in the presence of a strong laser field and a magnetic field of strength currently being used in laboratory experiments [9,11]. The electron energy and velocity components will also be shown as functions of the number of cycles $\eta/2\pi$ of the laser field. Let us first make the reminder that the laser-field propagation direction is the z axis. The added uniform magnetic field $\mathbf{B}_0$ also points in that direction. Hence the electric field component of the laser field will be along x and the magnetic field component will point along y.

Note as well that the case of an electron initially at rest at the origin may be studied using the same equations arrived at in this section, with β_0 set equal to zero everywhere. Such an electron will be accelerated from rest by the electric component of the laser field and will start moving in the negative x direction following turn-on of the laser. However, from that moment on the electron will start to ''feel'' the bending effects of the magnetic component of the laser field and $\mathbf{B}_0$. The former will tend to bend the electron trajectory around the y axis while the latter $\mathbf{B}_0$ will tend to make the electron follow a helix around the z axis. The net result is the helical trajectory shown in Fig. 1(a).

The general shape of the actual electron trajectory in the case of initial motion at a speed $c\beta_0$ along the z axis is the same. Due to the initial forward momentum, however, the electron, in this case, will describe a much longer helix over the same number of field cycles as in Fig. 1(a). The result for $\gamma_0=10$ ($\beta_0\approx 0.995$) and a set of field parameters similar to those of Fig. 1(a) is shown in Fig. 1(b). Note that the trajectory shown in Fig. 1(a) has been calculated for electron motion over 1000 laser field cycles, while that of Fig. 1(b) has been calculated over 100 such cycles only. As can be seen, the trajectory in Fig. 1(b) is not a perfect helix; there are wiggles due to the effect of the initial forward momentum. To a large forward velocity corresponds a large laser force magnetic component, comparable in magnitude to the electric component.

Extension of the electron trajectory in the transverse directions (x and y) is determined principally by the magnitude of the added magnetic field $\mathbf{B}_0$, while longitudinal extension (along z) depends mostly on the size of the electron initial speed β_0. The size of the wiggles, present in Fig. 1(b) but absent from Fig. 1(a), seems to be controlled by β_0 as well. Those wiggles are a manifestation of the bending effect due to the magnetic field component of the laser field. In order to better understand the electron motion, we have plotted the projection onto the xy plane of the trajectory shown in Fig. 1(b). In Fig. 1(c) this projection is shown over 100

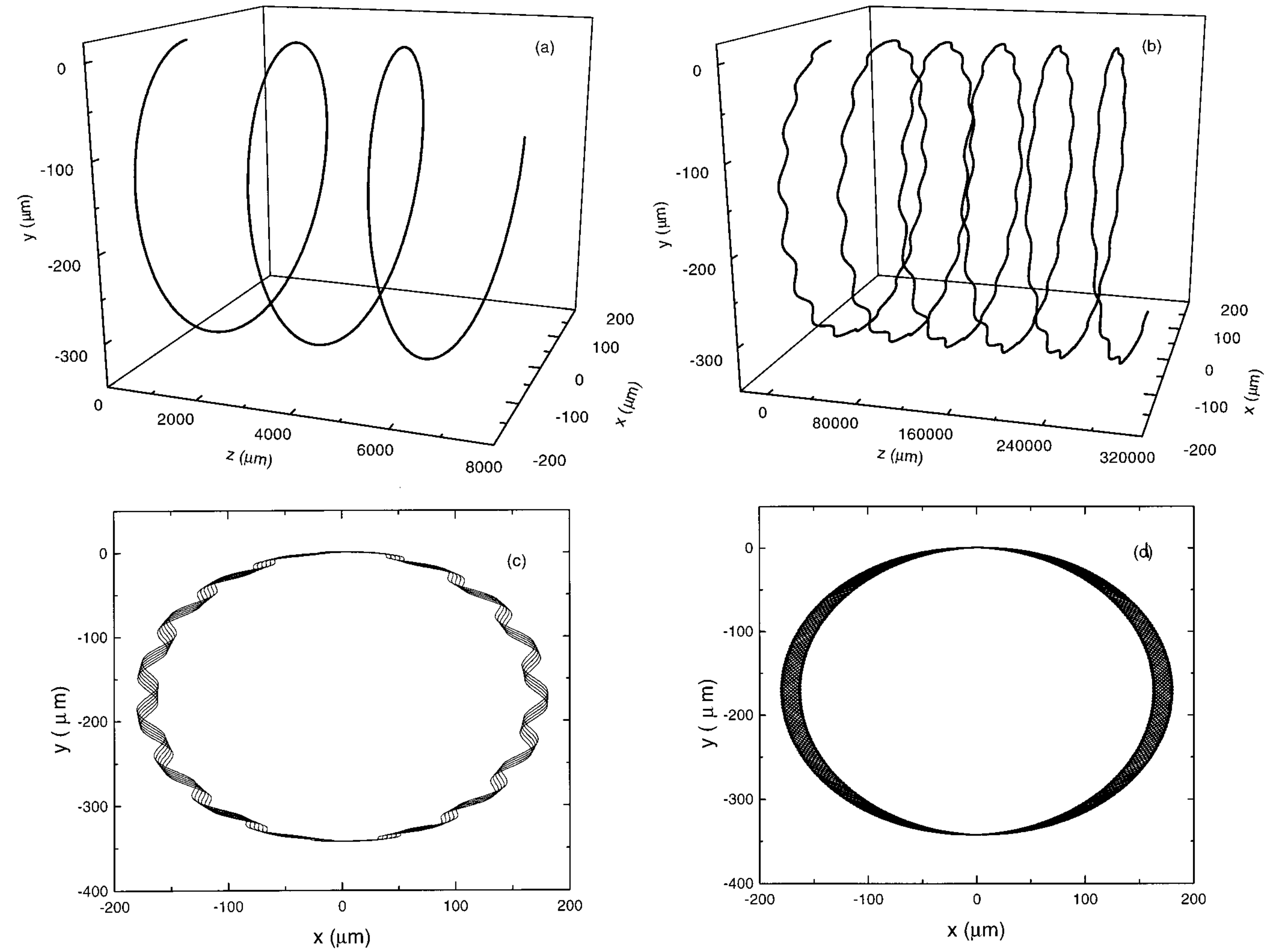

FIG. 1. Electron trajectory in the presence of a linearly polarized ($\delta=1$) superintense laser field propagating along the z axis, in addition to a strong uniform magnetic field of strength $B_0=30$ T, directed along z as well. The field parameters are intensity $q=3$ and wavelength $\lambda=1$ μm. (a) The electron is initially at rest, $\gamma=1$ or $\beta_0=0$. (b) The electron initially moves parallel to the laser propagation direction such that $\gamma_0=10$ or, equivalently $\beta_0\approx0.995$. (c) Projection onto the plane perpendicular to the laser propagation direction of the trajectory shown in (b). (d) A repeat of (c) over 500 laser field cycles. The trajectory in (a) is plotted over 1000 field cycles and in (b) and (c) over 100 cycles.

field cycles, while Fig. 1(d) shows the same projection, albeit over 500 cycles.

In Fig. 2 trajectories are shown for an electron moving under conditions identical to those of Fig. 1, but in a circularly polarized laser field. Figure 2(a) corresponds to Fig. 1(a) and so on. The two sets of trajectories corresponding to the two cases of field polarization share common features, in general.

The presence of the wiggles in the electron trajectory in Figs. 1(b) and 2(b) is also evidence for oscillations in the velocity of the electron. In Fig. 3 components of the scaled electron velocity are shown over 20 field cycles and for field parameters the same as those of Figs. 1 and 2. Note that the corresponding velocity components in the two polarization cases oscillate roughly between the same minima and maxima. In the case corresponding to a circularly polarized laser field, β_x and β_y [Figs. 3(d) and 3(e), respectively] exhibit beat structures, whereas β_z [Fig. 3(f)] oscillates between β_0 and a maximum value close to unity almost regularly.

In Fig. 4 we show the scaled electron energy γ as a function of the number of laser field cycles $\eta/2\pi$ for the same set of parameters used in Fig. 1 and over 20 laser field cycles. Notice that, in Fig. 4(a), the scaled energy oscillates (in fact, it exhibits a beat structure) between a maximum value of roughly 370 and a minimum value of 10, as has been remarked in the discussion following Eq. (29) above. In a circularly polarized field, on the other hand, the electron energy oscillates at the frequency $(1-r)\omega_0$ (corresponding equation not given in the text) between γ_0 and about 210. A comparison of the maxima in Figs. 4(a) and 4(b) reveals that the electron exchanges more energy with the linearly polarized field than it does with the circularly polarized field of the same intensity.

IV. RADIATION SPECTRA

The trajectory calculations made in Secs. II and III, interesting as they are in their own right, are essential for the study of radiation emitted by the accelerated electron. The starting point for calculating the angular and frequency distributions of the radiation is the radiant energy emitted per unit solid angle $d\Omega$ and per unit frequency interval $d\omega$ [16]

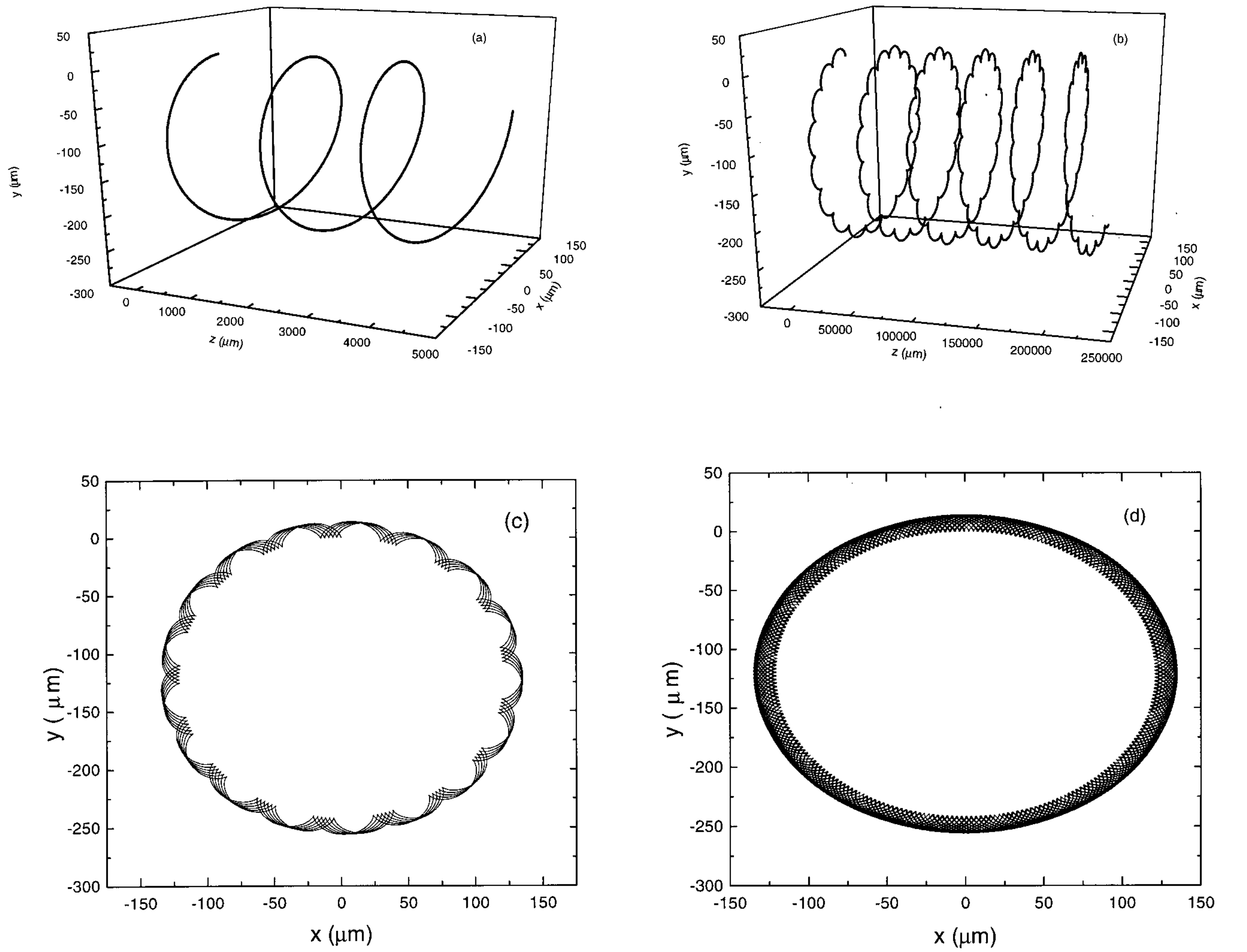

FIG. 2. Same as Fig. 1, but for a circularly polarized laser field.

$$\frac{d^2E(\omega,\Omega)}{d\Omega d\omega}=\frac{e^2}{4\pi^2c}\left|\int_0^T\frac{\mathbf{n}\times[\mathbf{n}-\boldsymbol{\beta}(t)]\times\dot{\boldsymbol{\beta}}(t)}{[1-\mathbf{n}\cdot\boldsymbol{\beta}(t)]^2}\right.$$
$$\left.\times\exp\left\{i\omega\left[t-\frac{\mathbf{n}\cdot\mathbf{r}(t)}{c}\right]\right\}dt\right|^2$$
$$=\frac{e^2}{4\pi^2c}\left|\left[\left(\frac{\mathbf{n}\times\mathbf{n}\times\boldsymbol{\beta}(t)}{1-\mathbf{n}\cdot\boldsymbol{\beta}(t)}\right)\right.\right.$$
$$\left.\times\exp\left\{i\omega\left(t-\frac{\mathbf{n}\cdot\mathbf{r}(t)}{c}\right)\right\}\right]_0^T$$
$$-i\omega\int_0^T[\mathbf{n}\times\mathbf{n}\times\boldsymbol{\beta}(t)]$$
$$\left.\times\exp\left\{i\omega\left(t-\frac{\mathbf{n}\cdot\mathbf{r}(t)}{c}\right)\right\}dt\right|^2. \quad (33)$$

E is used here to denote the radiated energy, $\mathbf{n}$ is a unit vector in the direction of propagation of the emitted radiation (direction of observation), and T is the time interval over which the incident field is nonzero. In the calculations used to produce the harmonic generation spectra to be reported below, we take $T=50$ field cycles. In order to make Eq. (33) easy to program, a change of integration variable has been made from t to η, in which case it is straightforward to show that the interval of integration changes from $(0,T)$ to $(0,100\pi)$.

For our purposes in this work, the harmonic generation spectrum will be given by the *doubly differential cross section*, obtained by dividing the radiant energy, emitted per unit solid angle per unit frequency and averaged over T, by the incident energy flux $(eq\omega_0)^2/8\pi cr_0^2$, r_0 being the classical electron radius. Thus

$$\frac{d^2\sigma(\omega,\Omega)}{d\Omega d\omega}=\frac{1}{T}\frac{8\pi cr_0^2}{(eq\omega_0)^2}\frac{d^2E(\omega,\Omega)}{d\Omega d\omega}. \quad (34)$$

The doubly differential cross section will be calculated on the basis of Eqs. (33) and (34) and will be plotted below against the scattered frequency, with the latter expressed in units of the laser frequency ω_0. Atomic units, with $e=m=1$, will be used.

Figures 5–7 give the spectra calculated numerically from Eqs. (33) and (34), corresponding to three different observation directions. Each set consists of five different plots, with

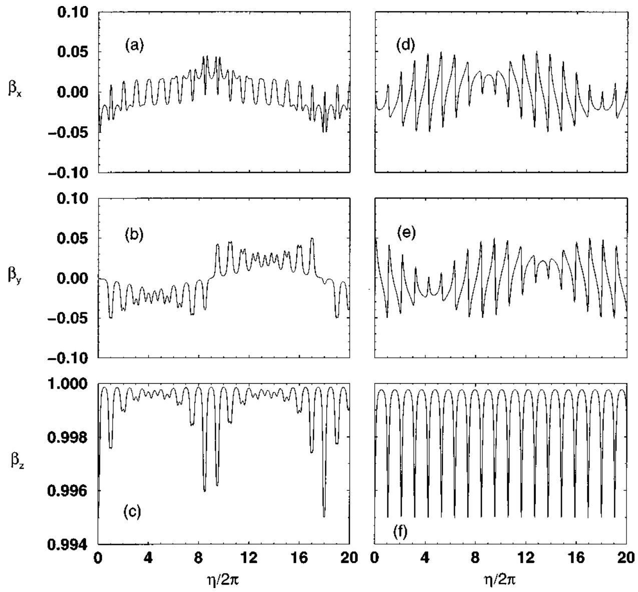

FIG. 3. Components of the scaled velocity vector of the electron whose trajectories are given in Figs. 1 and 2, shown here against the number of laser field cycles $\eta/2\pi$ over 20 such cycles. (a)–(c) Linearly polarized laser field and (d)–(f) circularly polarized laser field.

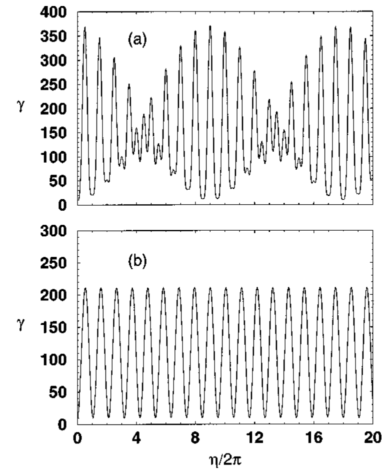

FIG. 4. Scaled electron energy vs $\eta/2\pi$ of the electron whose trajectories are given in Figs. 1 and 2, shown here over 20 field cycles. (a) Linearly polarized laser field and (b) circularly polarized laser field.

each plot corresponding to a specific set of values for the parameters ω_0, q, γ_0, and B_0. The parameter values are collected in Table I.

For example, the spectrum that would be observed along the laser propagation direction is shown in Fig. 5. Note that, in agreement with the analytical discussion given in Appendix A, the spectrum in this case consists of only two peaks. The main (Thomson) peak is located at $\omega=\omega_0$ in Figs. 5(a)–5(e), while the other (henceforth to be referred to as *the magnetic peak*, because it would be absent in the absence of the added uniform magnetic field B_0) moves from a position close to zero in Fig. 5(b) to nearly $\omega=5\omega_0$ in Fig. 5(d). In all cases, however, the position of the magnetic peak is determined by the value of the *ratio* r [cf Eq. (22)] which, in turn is proportional to both B_0 and γ_0. [In Fig. 5(d), $\gamma_0=1000$, while in Fig. 5(b), $\gamma_0=100$. Moreover, note that in Fig. 5(b), the magnetic peak is vanishingly small by comparison to the Thomson peak; it has also a vanishingly small frequency for the chosen set of parameters.] In general, the height of the magnetic peak increases with increasing electron initial kinetic energy, through a dependence upon γ_0; however, it seems to be insensitive, in Fig. 5 at least, to changes in the laser-field intensity or q. These two conclusions may be arrived at by studying the *approximate* equation (A10) and by comparing, e.g., Fig. 5(a) with Fig. 5(c). Nevertheless, it is difficult to draw similar conclusions on the basis of a similar analysis of the *exact* equation (33) or by comparing Figs. 6(a) and 7(a) with Figs. 6(c) and 7(c), respectively.

For a general observation direction, the spectrum is quite rich. According to Eq. (B10), the number of peaks to be expected is infinite. Note that the two peaks shown in Fig. 5 correspond to $(N,M)=(1,0)$ (Thomson) and (0,1) (magnetic).

Unfortunately, the general situation corresponding to an arbitrary observation direction does not lend itself to straightforward analytical scrutiny. In Appendix B we show that working analytically with Eq. (33) would involve many infinite sums over the product of as many ordinary Bessel functions. The analysis given in Appendix B is based on an approximate version of Eq. (33), in which $T\rightarrow\infty$ and the surface terms, the integrated part of Eq. (33), are dropped. We prefer to continue to work with the exact equation numerically. However, Appendix B does serve an important purpose: It shows clearly that one should expect an infinite number of peaks in the spectra corresponding to observation directions other than the forward one. This is also confirmed by the numerical investigations whose results are displayed graphically in Figs. 6 and 7.

For a set of parameters corresponding, one to one, to the set used in Fig. 5, we show harmonic generation spectra that would be observed along the electric (Fig. 6) and magnetic (Fig. 7) components of the laser field. In producing part (b) in each set, the aim has been to investigate the effect, on the spectrum, of changing the laser frequency from $\omega=0.05$ to 0.5 a.u. We only notice an approximately three-order-of-magnitude decrease in the relative peak heights as ω_0 is increased by one order of magnitude. We note, in this regard, that no regular basis exists for a *peak-to-peak* comparison. Similar arguments hold about changes in the general shapes of the spectra as one varies the magnitudes of the other parameters in a similar fashion.

In Figs. 8(a) and 8(b) we present magnified portions of the spectra shown in Figs. 6(a) and 7(a), respectively, in the

TABLE I. Parameter values used in Figs. 5–7.

Figure	ω_0 (a.u.)	q	γ_0	B_0 (T)
(a)	0.05	0.1	100	30
(b)	0.50	0.1	100	30
(c)	0.05	1.0	100	30
(d)	0.05	0.1	1000	30
(e)	0.05	0.1	100	40

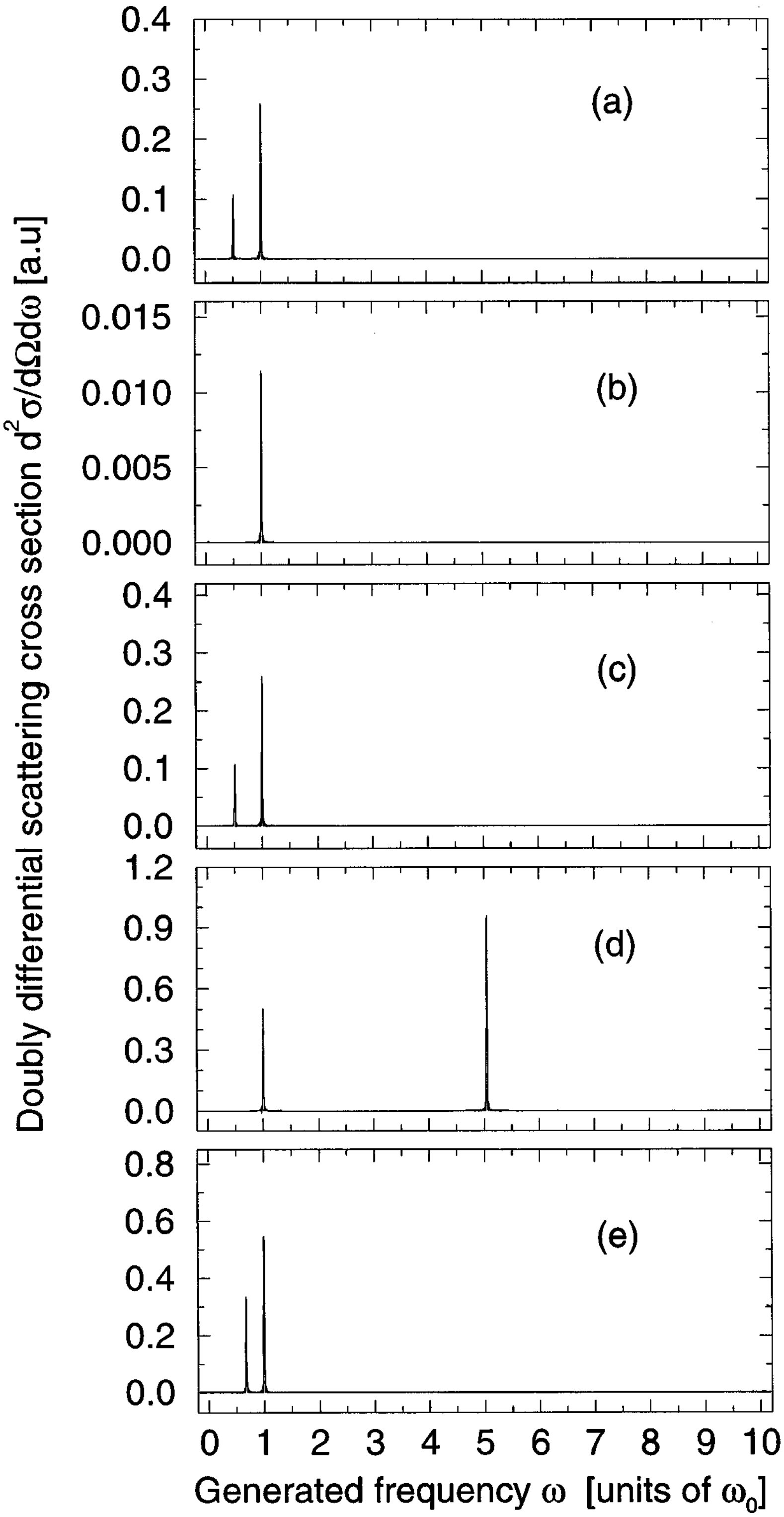

FIG. 5. Spectrum of the emitted radiation, in the presence of a laser field and a magnetic field, shown here in terms of the doubly differential scattering cross section, for observation along the laser propagation direction ($\theta=0$). The numerical integrations were carried out over 50 field cycles and the parameter set is given in Table I.

frequency region approximately between 16 ω_0 and $18\omega_0$. They show the presence of finite linewidths and substructures. Figures 7 and 8 strongly suggest that the emission spectra, observed in the direction of the electric- or the magnetic field components of the laser, have the nature of a chaotic radiation spectrum.

We close this section by noting that more and more pronounced peaks that correspond to higher and higher frequencies keep showing up in all the spectra. We have limited our investigations to a maximum harmonic order of 20, due to the fact that the calculation is very demanding in time. Production of harmonics of order beyond 20 may in principle be

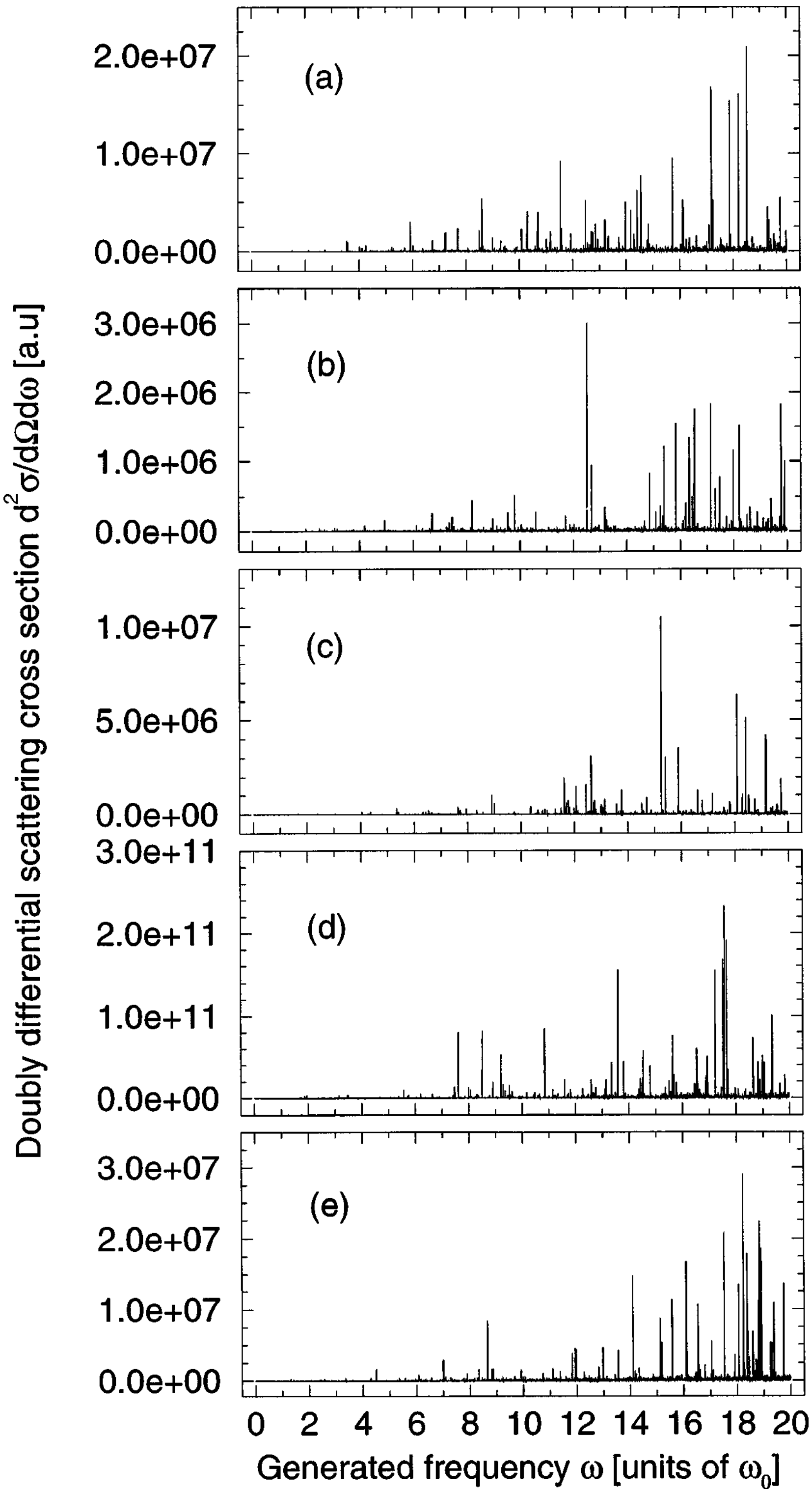

FIG. 6. Same as Fig. 5, but for observation along the magnetic component of the laser field ($\theta=\phi=\pi/2$).

done by employing computing power better than what is currently available to us. Moreover, resolution of adjacent peaks, in all of the spectra, except for the one observed in the forward direction, is difficult. This has an important implication with regard to the tunability of any device that may employ the underlying principle to generate high-frequency radiation.

V. SUMMARY

We have derived relativistic trajectory equations for a single electron in the presence of the combined effects of magnetic and laser fields, without any restrictions on the strength of the magnetic field, the intensity of the laser, or the initial direction of motion of the electron. We have shown that in a superintense laser field and a strong magnetic

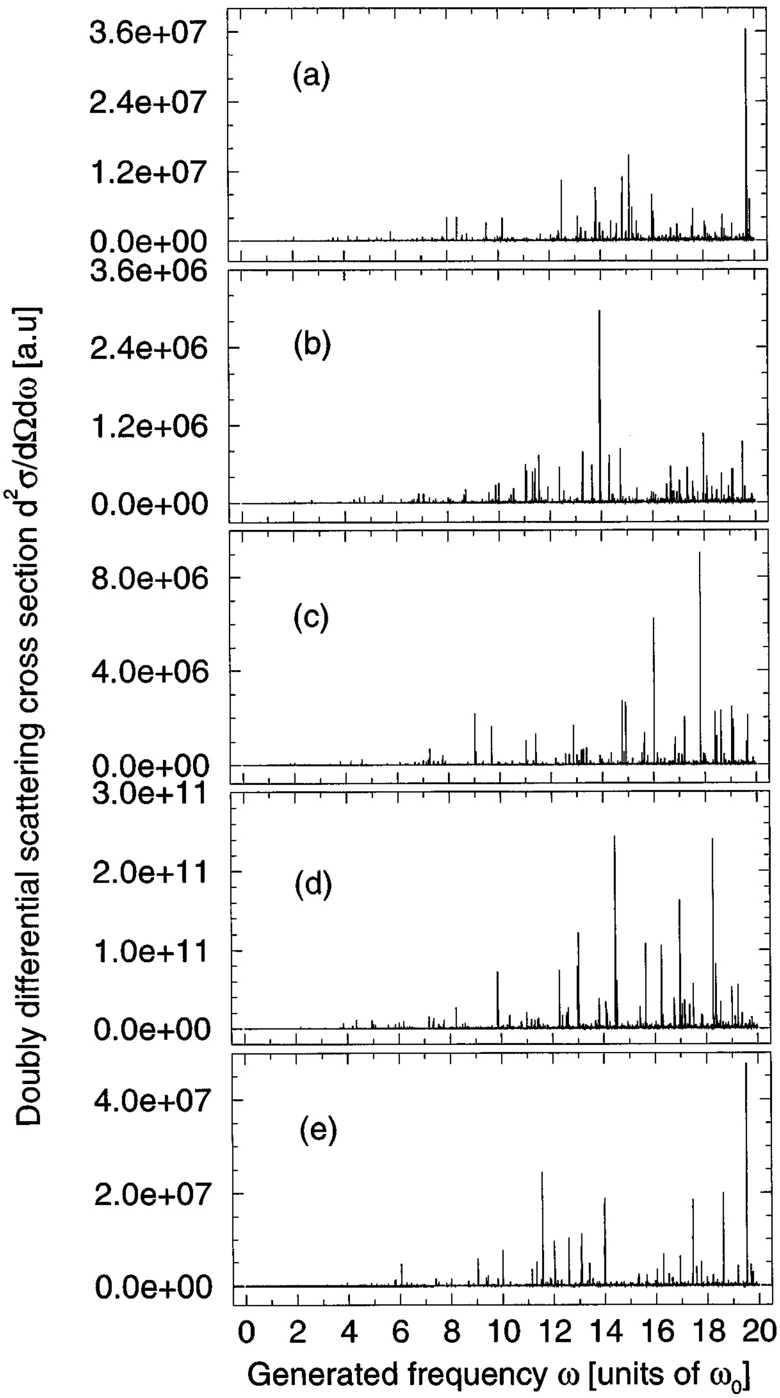

FIG. 7. Same as Fig. 5, but for observation along the electric component of the laser field ($\theta=\pi/2,\phi=0$).

field, the electron trajectory is a *rough* helix (with superimposed wiggles) around the common direction of the laser and magnetic fields.

Harmonic generation in the related problem has also been analytically investigated in a special case of electron initial motion parallel to the common directions of magnetic-field and laser propagation. In this restricted case, we have shown that radiation at a frequency depending upon the magnetic-field intensity, the laser frequency, and the electron initial speed, in addition to the familiar Thomson result, is generated. Numerical work, employing our trajectory equations, has also been carried out to study the generation of harmonics along other emission directions. The results have been shown in terms of the doubly differential scattering cross section for radiation observed along the electric and magnetic components of the laser field. In general, they show complex spectra with no regular pattern of positions and relative heights.

It is interesting to note that the present emission spectra differ from those found in Ref. [11], probably because of the

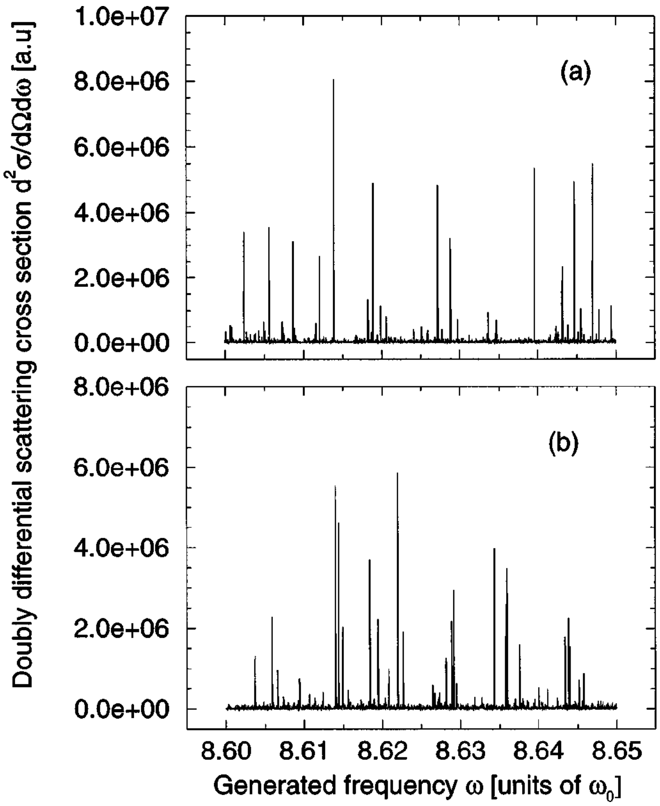

FIG. 8. Magnified portions of the spectra shown in Figs. 6(a) and 7(a).

very different form of the pulses employed (we use plane-wave fields with a sudden switch on/off, in contradistinction to a smooth pulse used in the above reference). We hope to study the dependence of the emission spectra on the pulse shape, as well as on the pulse duration, in greater detail in the future.

ACKNOWLEDGMENT

Y. I. S. acknowledges, with thanks, partial financial support for this work from the Alexander von Humboldt Stiftung.

APPENDIX A: EMISSION SPECTRUM IN THE FORWARD DIRECTION

In this appendix and the next, we employ an approximate version of Eq. (33), obtained by letting $T\to\infty$ and replacing the lower limit by $-\infty$ in order to make some analytic predictions about the number of Compton harmonics of the laser frequency that may be observed along a certain direction. We present details of the analysis of the case of observation along the forward direction first. In Appendix B the case of observation along an arbitrary direction will be briefly considered.

Although the laser turn-on time may be brief, if we let $T\to\infty$, Eq. (33) simplifies a great deal. First of all, the surface terms may be safely dropped and the resulting expression for the energy radiated per unit solid angle and per unit frequency will then become

$$\frac{d^2E}{d\Omega\, d\omega}=\frac{(e\omega)^2}{4\pi^2 c}\left|\int_{-\infty}^{\infty}[\mathbf{n}\times(\mathbf{n}\times\boldsymbol{\beta})]\exp\left\{i\omega\left(t-\frac{\mathbf{n}\cdot\mathbf{r}}{c}\right)\right\}dt\right|^2$$
$$=\frac{(e\omega)^2}{4\pi^2 c}\{|\mathbf{K}|^2-|\mathbf{n}\cdot\mathbf{K}|^2\}, \tag{A1}$$

where

$$\mathbf{K}=\int_{-\infty}^{\infty}\boldsymbol{\beta}(t)\exp\left[i\omega\left(t-\frac{\mathbf{n}\cdot\mathbf{r}(t)}{c}\right)\right]dt. \tag{A2}$$

Implied in the derivation of Eq. (A1) is the fact that only positive frequencies $\omega>0$ ought to be taken into account [16]. Let us confine our attention in the following analysis, to the relatively simple situation in which the point of observation lies on the z axis, i.e., $\mathbf{n}=\hat{\mathbf{k}}$; the analysis of more situations, involving other points of observation, will follow. In this case, Eqs. (A1) and (A2) take on a simple form and the integrations in Eq. (A2) may easily be carried out analytically. Equation (A1) becomes

$$\frac{d^2E}{d\Omega\, d\omega}=\frac{(e\omega)^2}{4\pi^2 c}\{|K_x|^2+|K_y|^2\}, \tag{A3}$$

where ($Q=x$ or y)

$$K_Q=\frac{1}{c}\int_{-\infty}^{\infty}\frac{dQ}{d\eta}e^{i(\omega/\omega_0)\eta}d\eta. \tag{A4}$$

In writing down Eq. (A4) from Eq. (A2), the integration variable has been changed from t to η. Using Eqs. (23) and (24) in Eq. (A4) and after some algebra, we obtain

$$K_x=\pi q\frac{\gamma_0(1+\beta_0)}{1-r^2}\{\delta(\omega-\omega_0)-\delta(\omega-r\omega_0)\}, \tag{A5}$$

$$K_y=i\pi q\frac{\gamma_0(1+\beta_0)}{1-r^2}\{r\delta(\omega-\omega_0)-\delta(\omega-r\omega_0)\}. \tag{A6}$$

Putting Eqs. (A5) and (A6) back into Eq. (A3), we obtain the expression for the energy per unit solid angle per unit frequency observed along the forward direction,

$$\frac{d^2E}{d\Omega\, d\omega}=\frac{(eq\omega)^2}{4c}\left[\frac{\gamma_0(1+\beta_0)}{1-r^2}\right]^2\{(1+r^2)[\delta(\omega-\omega_0)]^2$$
$$+2[\delta(\omega-r\omega_0)]^2\}. \tag{A7}$$

Thus the power P observed along the forward direction per unit solid angle per unit frequency may now be found [3]

$$\frac{d^2P}{d\Omega\, d\omega}=\frac{(eq)^2}{8\pi c}\left[\frac{\gamma_0(1+\beta_0)}{1-r^2}\right]^2\{(1+r^2)\omega^2\delta(\omega-\omega_0)$$
$$+2\omega^2\delta(\omega-r\omega_0)\}. \tag{A8}$$

Equation (A8) says that radiation at the frequencies ω_0 and $r\omega_0$ only will be observed in the forward direction. This agrees quite well with our *exact* numerical results displayed in Fig. 5. Expression (A8) may also be used to calculate the power observed per unit solid angle, by carrying out the integration over ω, with the result

$$\left(\frac{dP}{d\Omega}\right)_{lin}=\frac{(eq\omega_0)^2}{8\pi c}\left(\frac{1+\beta_0}{1-\beta_0}\right)\frac{1+3r^2}{(1-r^2)^2}. \qquad (A9)$$

Finally, when Eq. (A9) is divided by the incident flux $(eq\omega_0)^2/(8\pi c r_0^2)$, where r_0 is the classical electron radius, the formula for the scattering cross section of the radiation observed in the forward direction is obtained,

$$\frac{1}{r_0^2}\left(\frac{d\sigma}{d\Omega}\right)_{lin}=\left(\frac{1+\beta_0}{1-\beta_0}\right)\frac{1+3r^2}{(1-r^2)^2}. \qquad (A10)$$

The following expression, corresponding to the case of a circularly polarized laser field, may easily be obtained along the same lines:

$$\frac{1}{r_0^2}\left(\frac{d\sigma}{d\Omega}\right)_{cir}=\left(\frac{1+\beta_0}{1-\beta_0}\right)\frac{1+r^2}{(1-r)^2}. \qquad (A11)$$

Note that, in both cases of laser field polarization, for an electron initially at rest $\beta_0=0$ and in the absence of the added $\mathbf{B}_0$ field $r=0$, the physical situation corresponds to Thomson scattering. Under these conditions, Eqs. (A10) and (A11) yield $d\sigma/d\Omega=r_0^2$, as expected. We have also shown recently [1] that for nonzero initial velocity $\beta_0\neq 0$ and no magnetic field $\mathbf{B}_0=\mathbf{0}$,

$$\frac{1}{r_0^2}\frac{d\sigma}{d\Omega}=\frac{1+\beta_0}{1-\beta_0}. \qquad (A12)$$

Equations (A10) and (A11) have precisely this limit when the magnetic-field intensity is set equal to zero (or, equivalently, when $r\to 0$).

APPENDIX B: EMISSION SPECTRUM ALONG A GENERAL OBSERVATION DIRECTION

In this appendix we partially carry out the time integration in Eq. (A2) for a general observation direction. Let us take the observation direction along the unit vector $\boldsymbol{n}\equiv(n_1,n_2,n_3)=(\sin\theta\cos\phi,\sin\theta\sin\phi,\cos\theta)$. As a starting point, we rewrite Eq. (A2) in the form

$$\mathbf{K}=\int_{-\infty}^{\infty}\frac{d\mathbf{r}}{d\eta}\exp\left\{i\frac{\omega}{\omega_0}\left[\eta+\frac{\omega_0}{c}(z-\boldsymbol{n}\cdot\mathbf{r})\right]\right\}d\eta. \qquad (B1)$$

Next, we rewrite the parametric equations giving the electron trajectory, Eqs. (23)-(25), in the more compact form, for convenience,

$$x(\eta)=\frac{c}{\omega_0}A_1[r\sin\eta-\sin(r\eta)], \qquad (B2)$$

$$y(\eta)=\frac{c}{\omega_0}\{A_1[-r^2\cos\eta+\cos(r\eta)+r^2-1]\}, \qquad (B3)$$

$$z(\eta)=\frac{c}{\omega_0}\{A_2\eta+A_3\sin(2\eta) -A_4\sin[(1-r)\eta]-A_5\sin[(1+r)\eta]\}, \qquad (B4)$$

where

$$A_1=\frac{q}{r(1-r^2)}\gamma_0(1+\beta_0),$$

$$A_2=\frac{\beta_0}{1-\beta_0}+\frac{q^2}{4}\frac{3+r^2}{(1-r^2)^2}\frac{1+\beta_0}{1-\beta_0},$$

$$A_3=\frac{q^2/8}{1-r^2}\frac{1+\beta_0}{1-\beta_0}, \qquad (B5)$$

$$A_4=\frac{q^2}{2}\frac{(1+r)^2}{(1-r^2)^3}\frac{1+\beta_0}{1-\beta_0},$$

$$A_5=\frac{q^2}{2}\frac{(1-r)^2}{(1-r^2)^3}\frac{1+\beta_0}{1-\beta_0}.$$

Thus, for example,

$$K_x=\frac{c}{\omega_0}rA_1(I_1-I_2), \qquad (B6)$$

where

$$\begin{aligned}I_1&=\int_{-\infty}^{\infty}\cos\eta\exp\left[i\frac{\omega}{\omega_0}\left(\eta+\frac{\omega_0}{c}(z-\boldsymbol{n}\cdot\mathbf{r})\right)\right]d\eta,\\ &=\frac{1}{2}\int_{-\infty}^{\infty}d\eta\left\{\exp\left[i\left(1+\frac{\omega}{\omega_0}[1+(1-n_3)A_2]\right)\eta\right]\right.\\ &\quad\left.+\exp\left[i\left(-1+\frac{\omega}{\omega_0}[1+(1-n_3)A_2]\right)\eta\right]\right\}\\ &\quad\times\exp\left(i\frac{\omega}{\omega_0}[-a_0-a_1\sin\eta\right.\\ &\quad+a_2\sin r\eta+a_3\cos\eta-a_4\cos r\eta+a_5\sin 2\eta\\ &\quad\left.-a_6\sin(1-r)\eta-a_7\sin(1+r)\eta]\right),\end{aligned} \qquad (B7)$$

where $a_0=n_2(r^2-1)A_1$, $a_1=n_1rA_1$, $a_2=n_1A_1$, $a_3=n_2r^2A_1$, $a_4=n_2A_1$, $a_5=(1-n_3)A_3$, $a_6=(1-n_3)A_4$, and $a_7=(1-n_3)A_5$. I_2 involves $\cos r\eta$ instead of $\cos\eta$; otherwise it is structurally the same as I_1. Next, we express the second equality of Eq. (B7) as a product of Bessel function series according to the generating function

$$e^{ia\sin\theta}=\sum_{n=-\infty}^{\infty}J_n(a)e^{in\theta}. \qquad (B8)$$

The result will be a sevenfold sum involving the product of seven Bessel functions. The exponential terms in both lines of Eq. (B7), on the other hand, combine with the help of the well-known Bessel function recurrence relations into a single term containing the full η dependence, which then integrates immediately giving rise to a δ function. A similar result for I_2 may be obtained along similar lines. Finally, K_x becomes

$$K_x=2\pi c\left(\frac{\omega_0}{\omega}\right)\frac{rA_1}{[1+(1-n_3)A_2]}e^{-i(\omega/\omega_0)a_0}\sum_{j=-\infty}^{\infty}\sum_{k=-\infty}^{\infty}\sum_{l=-\infty}^{\infty}\sum_{m=-\infty}^{\infty}\sum_{n=-\infty}^{\infty}\sum_{p=-\infty}^{\infty}\sum_{s=-\infty}^{\infty}i^{m-n}\left(\frac{k}{a_1}-\frac{l}{a_2}\right)J_k\left(\frac{\omega a_1}{\omega_0}\right)J_l\left(\frac{\omega a_2}{\omega_0}\right)J_m\left(\frac{\omega a_3}{\omega_0}\right)J_n\left(\frac{\omega a_4}{\omega_0}\right)J_p\left(\frac{\omega a_5}{\omega_0}\right)J_j\left(\frac{\omega a_6}{\omega_0}\right)J_s\left(\frac{\omega a_7}{\omega_0}\right)\delta\left\{\omega-\left[\frac{N+rM}{1+(1-n_3)A_2}\right]\omega_0\right\}, \tag{B9}$$

where $N=k+m+j+s-2p$ and $M=s-(l+n+j)$ are integers such that $N+rM>0$. The same δ function may, in principle, be obtained when expressions similar to Eq. (B9) are found for K_y and K_z. Hence the scattered radiation will have a frequency given by

$$\omega^{(N,M)}=\left\{\frac{N+rM}{1+(1-\cos\theta)\left[\frac{\beta_0}{1-\beta_0}+\frac{q^2}{4}\frac{3+r^2}{(1-r^2)^2}\left(\frac{1+\beta_0}{1-\beta_0}\right)\right]}\right\}\omega_0,\quad N+rM>0. \tag{B10}$$

With N and M assuming positive and negative integer values, the condition expressed by Eq. (B10) may obviously be met by an infinite number of combinations. This manifests itself very clearly in the presence of an enormous number of peaks in the spectra shown in Figs. 6 and 7.

[1] Y. I. Salamin and F. H. M. Faisal, Phys. Rev. A **54**, 4383 (1996).
[2] Y. I. Salamin, J. Phys. A **30**, 4399 (1997).
[3] Y. I. Salamin and F. H. M. Faisal, Phys. Rev. A **55**, 3678 (1997).
[4] Y. I. Salamin and F. H. M. Faisal, Phys. Rev. A **55**, 3964 (1997).
[5] B. W. Boreham and H. Hora, Phys. Rev. Lett. **42**, 776 (1979).
[6] L. Cicchitelli, H. Hora, and R. Postle, Phys. Rev. A **41**, 3727 (1990).
[7] H. Hora, *Physics of Laser-Driven Plasmas* (Wiley, New York, 1981).
[8] S. Nakai, Laser Part. Beams **7**, 475 (1989); K. Mima, H. Tahabe, and S. Nakai, *ibid.* **7**, 249 (1989).
[9] C. H. Keitel and P. L. Knight, Phys. Rev. A **51**, 1420 (1995).
[10] J. Grotchmalicki, M. Lewenstein, M. Wilkens, and K. Rzazewski, J. Opt. Soc. Am. B **7**, 607 (1990).
[11] J.-P. Connerade and C. H. Keitel, Phys. Rev. A **53**, 2748 (1996).
[12] S. Foner and H. H. Kolm, Rev. Sci. Instrum. **27**, 547 (1956).
[13] E. S. Sarachik and G. T. Schappert, Phys. Rev. D **1**, 2738 (1970).
[14] G. A. Kyrala, J. Opt. Soc. Am. B **4**, 731 (1987).
[15] F. V. Hartemann, S. N. Fuchs, G. P. Le Sage, N. C. Luhmann, Jr., J. G. Woodworth, M. D. Perry, Y. J. Chen, and A. K. Kerman, Phys. Rev. E **51**, 4833 (1995).
[16] J. D. Jackson, *Classical Electrodynamics* (Wiley, New York, 1976).